Estimation of Wheel-Rail Adhesion Force Using Traction System Behavior

M. Moradi, R. Havangi *

Faculty of Electrical Engineering and Computer, University of Birjand, Birjand, Iran.

Article Info

Corresponding Author's Email Address:
Havangi@Birjand.ac.ir

Abstract

Background and Objectives: Traction system and adhesion between wheel and rail are fundamental aspects in rail transportation. Depending on the vehicle's running conditions, different levels of adhesion are needed. Low adhesion between wheel and rail can be caused by leaves on the line or other contaminants, such as rust or grease. Low adhesion can occur at any time of year especially in autumn, resulting in disruptions to passenger journeys. Increased wheel-rail adhesion for transit rail services results in better operating performance and system cost savings. Deceleration caused by low adhesion, will extend the braking distance, which is a safety issue. Because of many uncertain or even unknown factors, adhesion modelling is a time taking task. Furthermore, as direct measurement of adhesion force poses inherent challenges, state observers emerge as the most viable choice for employing indirect estimation techniques. Certain level of adhesion between wheel and rail leads to reliable, efficient, and economical operation.

Methods: This study introduces an advantageous approach that leverages the behavior of traction motors to provide support in achieving control over wheel slip and adhesion in railway applications. The proposed method aims to enhance the utilization of existing adhesion, minimize wheel deterioration, and mitigate high creep levels. In this regard, estimation of wheel-rail adhesion force is done indirectly by concentrating on induction motor parameters as railway traction system and dynamic relationships. Meanwhile, in this study, we focus on developing and applying the sixth-order Extended Kalman Filter (EKF) to create a highly efficient sensorless re-adhesion control system for railway vehicles.

Results: EKF based design is compared with Unscented Kalman Filter (UKF) based and actual conditions and implemented in Matlab to check the accuracy and performance ability for state and parameter estimation. Experimental results showed fast convergence, high precision and low error value for EKF.

Conclusion: The proposed technique has the capability to identify and assess the current state of local adhesion, while also providing real-time predictions of wear. Besides, in combination with control methods, this approach can be very useful in achieving high wheel-rail adhesion performance under variable complex road conditions.

Introduction

The contact force at wheel and rail interface governs the dynamic behavior of entire vehicle, which is complex and highly non-linear. Measurement of this force is one of the most important issues for condition monitoring and safety evaluation of railway vehicles. In [1] an estimator framework is presented for online identification of contact force at wheel- rail interface. Sliding and slipping are two challenging situations in railway industry that arise from the low friction between wheel and rail,

especially when wheel and rail are contaminated by different factors such as mud, grease, humidity, etc [2]-[5]. Also, weather conditions [6], deliberately applied friction modifiers [7], or contact surface temperatures [8]-[10], can affect the amount of adhesion. In order to avoid wheel slide/slip and uncomfortable riding and decrease in traction effort, wheel wear, and noise, it is imperative to minimize the excessive slippage that occurs between the surfaces of the wheel and the rail. In [11], the proposed method to reveal the slip is to compare speed difference between the wheel and the vehicle body. Then the estimated slip is used for torque compensation signal generation. Since the induction motor is one of the most important parts of the train's motion system, investigation of the induction motor was proposed which uses the estimated adhesion force to suppress the slip and adjust the torque command [12].

Many researchers tried to resolve adhesion problem and different solutions such as mathematical control theory, statistical and genetic have been proposed and applied [13], [14]. The adhesion characteristic has two stable and unstable areas. Between these two areas, maximum value of the adhesion is located. The adhesion coefficient depends upon the slip velocity, which influences on adhesion coefficient level. Train velocity and temperature of contact area are two important factors affecting the railway surfaces. Higher values of the adhesion coefficient and the slip velocity lead to maximum adhesion coefficient. Therefore, adhesion level identification is an important task for proper operation of a railway vehicle. A novel approach was introduced in a recent study [15] to determine the adhesion coefficient between the wheel and rail. Additionally, another research paper [16] presents a distinct adhesion control technique that relies on observing the adhesion state between the wheel and rail. Obtaining optimal adhesion control can lead to effective utilization of train traction power [17], [18]. It is important to mention that based on the changes observed in the characteristic curve of the adhesion coefficient, it is necessary to limit the creep velocity of the train within the stable region to prevent wheel slide or slip. To bring the trains back to the stable region, readhesion control is implemented by finely tuning the torque and promptly detecting instances of wheel slide or slip. However, a limitation of this approach is that it is unable to completely eliminate the occurrence of slide or slip [19]. To explore the phenomenon of slide and slip in railway traction, a novel approach utilizing the second-order Luenberger observer is introduced. This method indirectly determines the frictional force associated with this phenomenon [20]. A bank of Kalman Filter (KF) is applied for the adhesion estimation.

Identification of the contact conditions is then done by examining the residuals from the Kalman filters [21].

In [22] a Kalman Filter based technique is proposed for estimation of low adhesion between wheel and rail. The EKF is the nonlinear form of Kalman Filter, which has been used extensively for estimation of nonlinear states in navigation systems [23]. Extended Kalman filter based estimation for estimating the creepage, creep force, and friction coefficient between the wheel and rail surfaces by utilizing the AC motor parameters such as stator voltage, current, and speed was proposed in [24]. An alternative approach to detect slip velocity is through the utilization of multi-rate Extended Kalman Filter state identification. This method combines both the multi-rate technique and the EKF method to accurately determine the traction motor load torque. The advantages of this method are faster slip detection and improved reliability and traction performance [25]. To predict the wheel and rail wear, regions of adhesion variations or low adhesion, and the development of rolling contact fatigue, a novel approach utilizing the Kalman-Bucy filter technique is suggested to estimate the wheel and the rail states [26]. In [27], a model-based technique is proposed for condition monitoring, in which an unscented Kalman filter is applied to estimate rolling radius by considering the angular velocity and the traction effort of the motor measurements. In [28]-[30] UKF was used for sensorless speed control of induction motor, in which it was emphasized that UKF has more robust estimation performance.

This study investigates the utilization of EKF approach to accurately determine the adhesion force between the contact surfaces of a wheel and rail. The estimation is achieved through analyzing the measured values of the stator currents of an induction motor. To evaluate the observer's performance, a dynamic model is constructed, comprising a gear box, wheelset, and induction motor. The behavior of the wheel-rail contact is described using the Polach model. The design of the induction motor is based on a first-order decomposition of the sixth-order nonlinear model. The proposed EKF technique is capable of estimating various parameters, including motor current, rotor flux components, motor speed, and load torque.Then, dynamic reletion is used for adhesion force estimation. For further investigation, we compared our method with UKF. The obtained results show good convergence and high precision. The rest of this research is organized into four parts. First, the details of traction system and mathematical model of induction motor are explained. Then, the estimator framework is presented. Following this, the details of experimental results are highlighted. Finally, the conclusion is given.

System Modelling and Discretization

The traction system information employed in this research is shown in Fig. 1. The model consists of three parts, wheel and rail, gear wheel, and traction motor. The

continuous dynamic model of the induction motor used in this research is described by sixth-order nonlinear differential equations with three series of variables consisting of two mechanical variables (motor speed and load torque), four electrical variables (currents and fluxes), and two control variables (stator voltages) and the stationary reference frame is (α, β).   The action of the axle load causes the wheels rotation, which leads to micro deformation region occurring in the wheel-rail contact region. Then, the interaction between wheel and rail produces the adhesion force F_a. The schematic of wheel-rail adhesion mechanism is shown in Fig. 2. The states, the measurements, the stator voltages, and the state and measurement noises are given in (1) to (5) respectively.
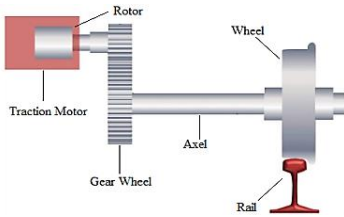
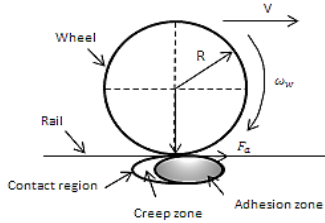
Fig. 1: Schematic of the traction system.

Fig. 2: Wheel-rail adhesion mechanism.

$$x(t) = [x_1 \quad x_2 \quad x_3 \quad x_4 \quad x_5 \quad x_6]^T =$$
$$[I_{s\alpha} \quad I_{s\beta} \quad \psi_{r\alpha} \quad \psi_{r\beta} \quad \omega_m \quad T_L]^T \quad (1)$$

$$z = [I_{s\alpha} \quad I_{s\beta}]^T \quad (2)$$

$$u(t) = [u_{s\alpha} \quad u_{s\beta}]^T \quad (3)$$

$$w(t) = [w_1 \quad w_2 \quad w_3 \quad w_4 \quad w_5 \quad w_6]^T \quad (4)$$

$$v = [v_1 \quad v_2]^T \quad (5)$$

where $I_{s\alpha}$ is stator current in α frame, $I_{s\beta}$ is stator current in β frame, $\psi_{r\alpha}$ is rotor flux in α frame, $\psi_{r\beta}$ is rotor flux in β frame, ω_m is the motor angular velocity, and T_L is load torque.

The equations are listed as follows [31]:

$$\frac{dI_{s\alpha}}{dt} = -\left(\frac{R_s}{\sigma L_s} + \frac{L_m^2 R_r}{\sigma L_s L_r^2}\right) I_{s\alpha} + \frac{L_m R_r}{\sigma L_s L_r^2} \psi_{r\alpha} +$$
$$\frac{L_m}{\sigma L_s L_r} n_p \omega_m \psi_{r\beta} + \frac{1}{\sigma L_s} u_{s\alpha} \quad (6)$$

$$\frac{dI_{s\beta}}{dt} = -\left(\frac{R_s}{\sigma L_s} + \frac{L_m^2 R_r}{\sigma L_s L_r^2}\right) I_{s\beta} - \frac{L_m}{\sigma L_s L_r} n_p \omega_m \psi_{r\alpha} +$$
$$\frac{L_m R_r}{\sigma L_s L_r^2} \psi_{r\beta} + \frac{1}{\sigma L_s} u_{s\beta} \quad (7)$$

$$\frac{d\psi_{r\alpha}}{dt} = \frac{R_r L_m}{L_r} I_{s\alpha} - \frac{R_r}{L_r} \psi_{r\alpha} - n_p \omega_m \psi_{r\beta} \quad (8)$$

$$\frac{d\psi_{r\beta}}{dt} = \frac{R_r L_m}{L_r} I_{s\beta} + n_p \omega_m \psi_{r\alpha} - \frac{R_r}{L_r} \psi_{r\beta} \quad (9)$$

$$\frac{d\omega_m}{dt} = \frac{-3 n_p L_m}{2 J_{eqv} L_r} \psi_{r\beta} I_{s\alpha} + \frac{3 n_p L_m}{2 J_{eqv} L_r} \psi_{r\alpha} I_{s\beta} - \frac{C_v}{J_{eqv}} \omega_m - \frac{1}{J_{eqv}} T_L \quad (10)$$

$$\frac{dT_L}{dt} = 1 \quad (11)$$

where R_s is the stator resistance, R_r is the rotor resistance, L_s is the stator self-inductance, L_r the is rotor self-inductance, L_m is the mutual inductance, n_p is the number of the pole pairs, J_{eqv} is the equivalent moment of inertia, C_v is the viscous friction, and σ is the leakage coefficient and defined as (12).

$$\sigma = 1 - \frac{L_m^2}{L_s L_r} \quad (12)$$

Induction motor extended model is shown in (13).

$$\underbrace{\begin{bmatrix} \dot{i}_{s\alpha} \\ \dot{i}_{s\beta} \\ \dot{\psi}_{r\alpha} \\ \dot{\psi}_{r\beta} \\ \dot{\omega}_m \\ \dot{T}_L \end{bmatrix}}_{\dot{x}_e} = \underbrace{\begin{bmatrix} -\left(\frac{R_s}{\sigma L_s} + \frac{L_m^2 R_r}{\sigma L_s L_r^2}\right) & 0 & \frac{L_m R_r}{\sigma L_s L_r^2} & \frac{L_m}{\sigma L_s L_r} n_p \omega_m & 0 & 0 \\ 0 & -\left(\frac{R_s}{\sigma L_s} + \frac{L_m^2 R_r}{\sigma L_s L_r^2}\right) & -\frac{L_m}{\sigma L_s L_r} n_p \omega_m & \frac{L_m R_r}{\sigma L_s L_r^2} & 0 & 0 \\ \frac{R_r L_m}{L_r} & 0 & -\frac{R_r}{L_r} & -n_p \omega_m & 0 & 0 \\ 0 & \frac{R_r L_m}{L_r} & n_p \omega_m & -\frac{R_r}{L_r} & 0 & 0 \\ \frac{-3 n_p L_m}{2 J_{eqv} L_r} \psi_{r\beta} & \frac{3 n_p L_m}{2 J_{eqv} L_r} \psi_{r\alpha} & 0 & 0 & -\frac{C_v}{J_{eqv}} & -\frac{1}{J_{eqv}} \\ 0 & 0 & 0 & 0 & 0 & 1 \end{bmatrix}}_{A_e} \underbrace{\begin{bmatrix} I_{s\alpha} \\ I_{s\beta} \\ \psi_{r\alpha} \\ \psi_{r\beta} \\ \omega_m \\ T_L \end{bmatrix}}_{x_e} + \underbrace{\begin{bmatrix} \frac{1}{\sigma L_s} & 0 \\ 0 & \frac{1}{\sigma L_s} \\ 0 & 0 \\ 0 & 0 \\ 0 & 0 \\ 0 & 0 \end{bmatrix}}_{B_e} \underbrace{\begin{bmatrix} U_{s\alpha} \\ U_{s\beta} \end{bmatrix}}_{U_e} + w(t) \quad (13)$$

$$\underbrace{\begin{bmatrix} I_{s\alpha} \\ I_{s\beta} \end{bmatrix}}_{Z} = \underbrace{\begin{bmatrix} 1 & 0 & 0 & 0 & 0 & 0 \\ 0 & 1 & 0 & 0 & 0 & 0 \end{bmatrix}}_{H_e} \begin{bmatrix} I_{s\alpha} \\ I_{s\beta} \\ \psi_{r\alpha} \\ \psi_{r\beta} \\ \omega_m \\ T_L \end{bmatrix} + v(t) \quad (14)$$

Ignoring the damping coefficient, the dynamic equation of traction motor is as follows [13]:

$$\frac{d\omega_m}{dt} = \frac{T_m - T_L}{J_{eqv}} \quad (15)$$

$$\omega_w = \frac{\omega_m}{n_i} \quad (16)$$

$$T_m = \frac{n_p L_m}{L_r}(I_{s\beta}\psi_{r\alpha} - I_{s\alpha}\psi_{r\beta}) \tag{17}$$

$$T_L = \frac{2rF_a}{n_i} \tag{18}$$

$$J_{eqv} = J_m + \frac{J_g + J_x + J_{wR} + J_{wL}}{n_i^2} \tag{19}$$

where ω_w represents the angular velocity of the wheel, while Fa denotes the adhesion force exerted by a single wheel. Additionally, J_m, J_g, J_x, J_{wR}, and J_{wL} refer to the moments of inertia associated with the motor, gearbox, wheelset axle, right wheel, and left wheel, respectively. The adhesion force at the contact point between the wheel and rail, denoted as F_a is determined using Polach's method [33] and can be calculated using (20).

$$F_a = \frac{2F_N\mu_f}{\pi}\left(\frac{k_A\epsilon}{1+(k_A\epsilon)^2} + \arctan(k_S\epsilon)\right), \ k_S \le k_A \le 1 \tag{20}$$

where F_N is the normal force between the wheel and rail, μ_f is the traction coefficient, and quantities k_A and k_S are Polach reduction factors in the areas of adhesion and slip, respectively.

$$\mu_f = \mu_0((1-D)e^{-B\xi V} + D) \tag{21}$$

$$\epsilon = \frac{G\pi a b C_{11}}{4F_N\mu_f}\xi \tag{22}$$

where D and B represent reduction factors associated with distinct friction coefficients, V is the longitudinal velocity of the train, ξ is the creepage between the wheel and rail, G is shear module, a and b are the semi-axis length of the contact patch and C_{11} is the Kalker coefficient.

The creepage contains longitudinal and lateral components but in this research, the lateral dynamics are neglected, so calculated by the following equation [34]:

$$\xi = \frac{\omega_w r - V}{V} \tag{23}$$

Estimation of Wheel-Rail Adhesion

The details of the EKF and UKF used for estiomation of Wheel-Rail adhesion can be found in the following subsections.

A. Extended Kalman Filter

The EKF is an enhanced variant of the traditional Kalman filter that takes into account nonlinear systems. In this study, our goal is to determine the optimal linear estimation for the state vector of the induction motor. The discrete-time nonlinear model is expressed as below:

$$x_{k+1} = f(x_k, u_k, w_k) \tag{24}$$

$$z_k = h(x_k, v_k) \tag{25}$$

where $f(.)$ represents the dynamics of machine, $h(.)$ is the relationship between the observation z_k and the state vector x_k, u_k refers to the input provided to the motor, while w_k and v_k represent the vectors of noise that affect the process and measurement respectively. Equations (24) and (25) exhibit nonlinearity, necessitating their linearization. This process involves employing the first-order Taylor approximation in the vicinity of a chosen reference point. Linearizing these nonlinear equations will result in the following description of the dynamics:

$$x_{k+1} = f(\hat{x}_k, u_k, 0) + F_K(x_k - \hat{x}_k) + W_k w_k \tag{26}$$

$$z_k = h(\hat{x}_k, 0) + H_K(x_k - \hat{x}_k) + V_k(v_k - 0) \tag{27}$$

where F_K, W_k, H_K and V_k are Jacobean matrices defined as below:

$$F_K = \frac{\partial f}{\partial x}\Big|_{\hat{x}_k}, W_k = \frac{\partial f}{\partial w}\Big|_w, H_K = \frac{\partial h}{\partial x}\Big|_{\hat{x}_k}, V_k = \frac{\partial h}{\partial v}\Big|_{\hat{x}_k} \tag{28}$$

The EKF algorithm using induction motor model in (13) and (14) can be given by the following equations:

$$P_{k+1|k} = F_K P_k(k) F_K^T + W_k Q W_K^T \tag{29}$$

$$K_K = P_{k+1|k} H_k^T (H_k P_{k+1|k} H_k^T + V_k R V_K^T)^{-1} \tag{30}$$

$$\hat{x}_{k+1|k} = f(\hat{x}_{k|k}, u_k, 0) \tag{31}$$

$$\hat{x}_{k+1|k+1} = \hat{x}_{k+1|k} + K_K(z_k - h(\hat{x}_{k+1|k}, 0)) \tag{32}$$

$$P_{k+1|k+1} = (I - K_K H_k) P_{k+1|k} \tag{33}$$

where $P_{k+1|k}$ is the priori prediction error covariance matrix, $P_{k+1|k+1}$ is the posteriori prediction error covariance matrix, K_K is the Kalman gain, $\hat{x}_{k+1|k}$ is the priori state prediction vector, $\hat{x}_{k+1|k+1}$ is the posteriori state prediction vector and Q and R are the covariance matrixes of process and measurement noise and I is the unit matrix symbol. In general, the extended Kalman filter is not an optimal estimator. If the process is modeled incorrectly, or if the initial estimate of the state is wrong, linearization may lead to rapid divergence of the filter. Furthermore, the estimated covariance matrix in EKF has a tendency to inaccurately assess the true covariance matrix. Consequently, it runs the risk of losing consistency in the statistical context unless stabilizing noise is introduced. Finally, because of the Q and R uncertainty, their values are obtained by trial-and-error methods which is tedious and time-consuming procedure.

B. Unscented Kalman Filter

The UKF is created by incorporating the unscented transformation (UT) method. It is assumed that the studied system is nonlinear and in discrete form:

$$x_k = f(\hat{x}_k, u_k) + w_k \qquad w_k \sim (0, Q_k) \tag{34}$$

$$z_k = h(\hat{x}_k, u_k) + v_k \qquad v_k \sim (0, R_k) \tag{35}$$

In the first step of estimate of state vector of the induction motor using UKF, a set of $2n_x + 1$ weighted samples or sigma points are determined as:

$$\chi_{k-1} = [\hat{x}_{k-1} \quad \hat{x}_{k-1} + \sqrt{(n_x + \lambda)(P_{k-1})_i} \quad \hat{x}_{k-1} - \sqrt{(n_x + \lambda)(P_{k-1})_i}] \tag{36}$$

274

J. Electr. Comput. Eng. Innovations, 12(1): 271-282, 2024

$$w_m^{(0)} = \frac{\lambda}{\lambda + n_x} \tag{37}$$

$$w_c^{(0)} = \frac{\lambda}{\lambda + n_x} + 1 - \alpha^2 + \beta \tag{38}$$

$$w_c^{(j)} = w_m^{(j)} = \frac{\lambda}{2(\lambda + n_x)} \tag{39}$$

where the dimension of the state variable is represented as n_x. The estimate of x_k at time k-1 is denoted as $\hat{x}_{k-1}$, and its covariance is represented as P_{k-1}. The weight w_m is is utilized for determining the mean, while w_c is employed for calculating the covariance. The parameter α, which lies within the range of [0,1], is employed to regulate the distribution of the sigma points. Additionally, β non-negative term, is utilized to incorporate information from higher order moments of the distribution and $\lambda = \alpha^2(n_x + \rho) - n_x$. It should be noted that in this study, these three parameters are set as follows: $\alpha = 1$, $\beta = 0$ and $\rho = 1$

The column i of the matrix P_{k-1} is denoted as $(P_{k-1})_i$. Sigma points χ_{k-1} are substituted into the nonlinear state equation, and the transformed sigma points are evaluated for each of the the 0 - $2n_x$ points as described below:

$$\chi_k^{(i)} = f(\chi_{k-1}^{(i)}, u_k) \tag{40}$$

To obtain the mean and covariance of the modified set of sigma points, the following procedure is employed:

$$\hat{x}_k^- = \sum_{i=1}^{2n_x} w_m^{(i)} \chi_k^{(i)} \tag{41}$$

$$P_k^- = \sum_{i=1}^{2n_x} w_c^{(i)} (\chi_k^{(i)} - \hat{x}_k^-)(\chi_k^{(i)} - \hat{x}_k^-)^T + Q_k \tag{42}$$

where Q_k is the process noise covariance. The sigma points that have been transformed are subsequently utilized to predict the measurements by employing the measurement model:

$$\xi^{(i)} = h(\chi_k^{(i)}, U_k) \tag{43}$$

The expected measurement $\hat{z}_k$ is as:

$$\hat{z}_k = \sum_{i=1}^{2n_x} w_m^{(i)} \xi^{(i)} \tag{44}$$

Using the predicted sigma points, P_k^{xz} and P_k^{zz} also determines as follows:

$$P_k^{xz} = \sum_{i=0}^{2n} \omega_i^{(c)} (\chi_k^{(i)} - \hat{x}_k)(\xi^{(i)} - \hat{z}_k^-)^T \tag{45}$$

$$P_k^{zz} = \sum_{i=0}^{2n} \omega_i^{(c)} (\xi^{(i)} - \hat{z}_k^-)(\xi^{(i)} - \hat{z}_k^-)^T + R_k \tag{46}$$

The mean and square root of covariance for the state are recalculated based on the actual measurement.

$$\hat{x}_k = \hat{x}_k + K_k(z_k - \hat{z}_k) \tag{47}$$

$$P_k = P_k^- - K_K P_k^{xz} K_K^T \tag{48}$$

$$K_k = P_k^{xz}(P_k^{zz})^{-1} \tag{49}$$

Results

This section begins by simulating the presented model to verify the accuracy of the EKF in estimating variables. Subsequently, the performance of the EKF is assessed by comparing it with the UKF to determine its accuracy as an estimator. All of our codes have been developed and implemented using the Matlab, with a sampling period of 10^{-3}s seconds. To ensure more realistic testing conditions, the induction motor is powered through an AC drive with a sinusoidal input voltage.

A. EKF-Based Model Simulation

In the first step of our simulation, we try to simulate contact conditions. Our goal in this step is to show the created changes in adhesion force versus creepage for all track conditions such as dry, wet, low, and very low relationship between adhesion force and creepage. The designed friction coefficients are as follows:

$$\mu_0 = \begin{cases} 0.55 & t < 10 \\ 0.3 & 10 \leq t < 20 \\ 0.06 & 20 \leq t < 30 \\ 0.03 & 30 \leq t < 35 \end{cases}$$

The values of k_A, k_S, D and B under different friction conditions are listed in Table 1 and the other parameter values used in equations (20) to (23) are as the following: F_N = 60 KN, G = 8.4×10^{10} $\frac{N}{m^2}$, a = 0.0015 m, b = 0.0075 m, C_{11} =4.12, V= 15 $\frac{m}{s}$

Fig. 3 shows the curves of the adhesion force versus creepage in different wheel-rail contact conditions. As the creepage increases, the slip region increases versus the stick region. As we see, the adhesion force changes with respect to creepage for all track conditions nonlinearly. In the second step, the results of the simulation in MATLAB and the estimation of the variables mentioned in the previous section are shown and discussed.

Table 1: Polach model parameters under different friction conditions [24]

Model parameter	Wheel–rail conditions			
	Dry	Wet	Low	Very Low
k_A	1	1	1	1
k_S	0.4	0.4	0.4	0.4
D	0.6	0.2	0.2	0.1
B	0.4	0.4	0.4	0.4

The parameter values for the traction system employed in this research can be found in Table 2.

Matrices Q and R are given in the following, which are obtained by trial and error.

Q = diag ([3.88e-7 1.00e-12 1.39e-16 1.42e-16 1.85e-10 1.85e-3]) × 0.099, R = diag ([3.39e-4 3.39e-4]) × 2.

Table 2: Parameters and values used in the simulation

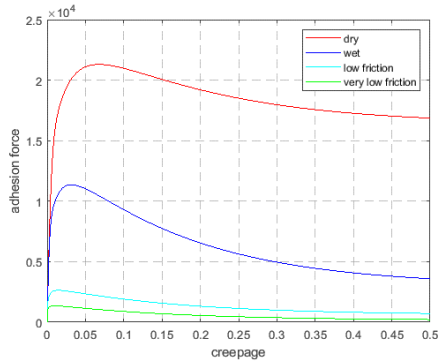|			
C_v ($\frac{N.m}{rad.s}$)	0.015	J_{eqv} (kg.m²)	0.07
L_S(H)	0.1004	R_S (Ω)	1.54
L_m(H)	0.0915	R_r (Ω)	1.294
L_r(H)	0.0969	r (m)	0.34
n_i	7.5	f (Hz)	50
n_p	3		

Fig. 3: Adhesion force curves creepage.

Estimated and actual trajectories of stator currents in α and β frames ($\hat{I}_{s\alpha}, \hat{I}_{s\beta}$) are shown in Fig. 4 (a) and (b), respectively. The trajectories of the current errors in α and β frames ($e_{I_{s\alpha}}, e_{I_{s\beta}}$) are represented in Fig. 5 (a) and (b), respectively.
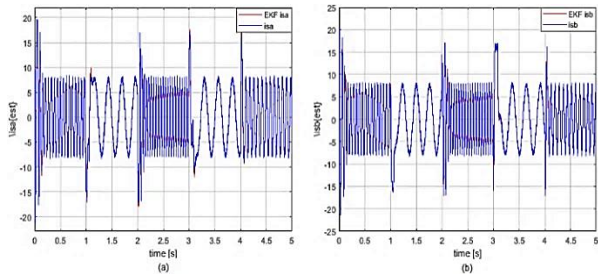
Fig. 4: EKF based estimated and actual motor current trajectories (a) α axis (b) β axis.
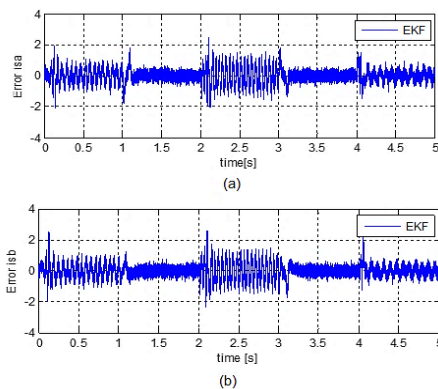
Fig. 5: The trajectories of the motor current error (a) α axis (b) β axis.

Estimated and actual trajectories of rotor fluxes in α and β frames ($\hat{\psi}_{r\alpha}, \hat{\psi}_{r\beta}$) are represented in Fig. 6 (a) and (b), respectively. The trajectories of the rotor flux errors in α and β frames ($e_{\psi_{s\alpha}}, e_{\psi_{s\beta}}$) are represented in Fig. 7 (a) and (b), respectively.

As seen in Fig. 4 (a) and (b) and Fig. 6 (a) and (b), the estimated trajectories of the stator current and rotor flux in α and β frames follow the real trajectories of these four motor variables with minimal error bound.

Estimated and actual trajectories of motor speed (ω_m, $\hat{\omega}_m$) and speed error (e_{ω_m}) are shown in Figs. 8 and 9 respectively. In Fig. 8, fast convergence with a very low bound of error in following the real trajectory by the EKF estimator is clearly evident. The trajectories of the estimated and actual load torque ($T_L, \hat{T}_L$) and load torque error (e_{T_L}) are given in Figs. 10 and 11 respectively.
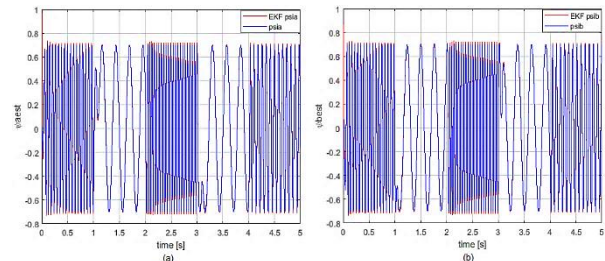
Fig. 6: EKF based estimated and actual rotor flux trajectories (a) α axis (b) β axis.

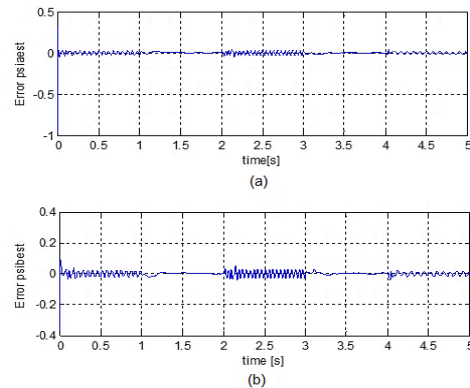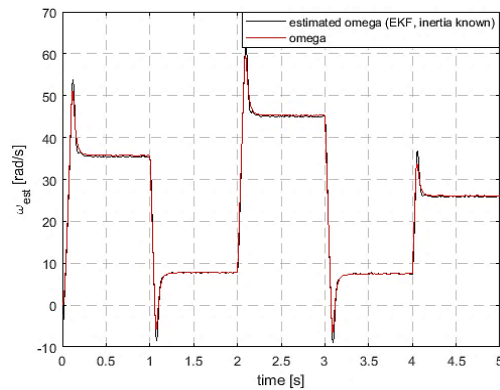Fig. 7: The trajectories of the rotor fluxes error (a) α axis (b) β axis.

Fig. 8: EKF based estimated and actual trajectories of motor speed.
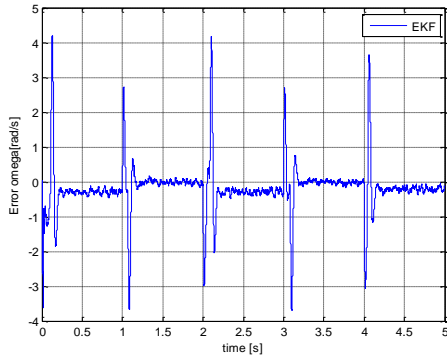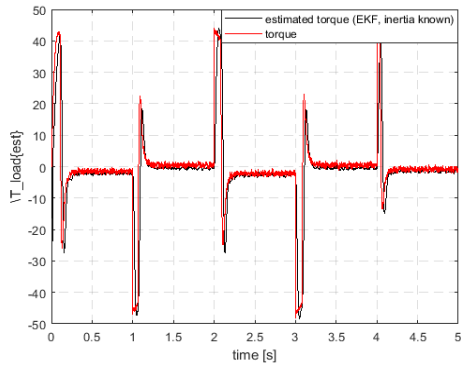
Fig. 9: The trajectory of the motor speed error.

Fig. 10: EKF based estimated and actual trajectories of load torque.
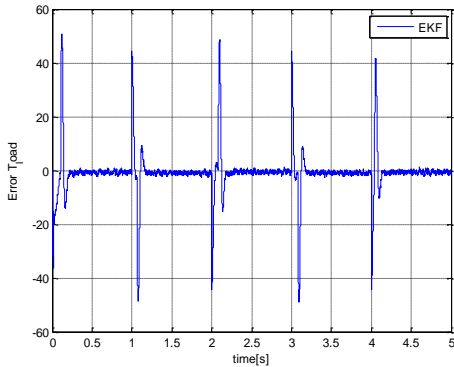

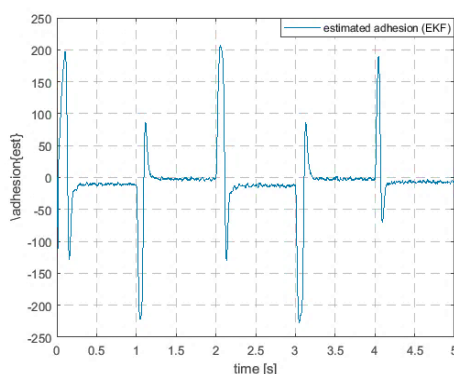Fig. 11: The trajectory of the load torque error.

Fig. 12. The trajectory of the estimated adhesion force.

Referring to Fig. 10, it is evident that the error undergoes a narrow variation when there is a sudden change in the torque command. By analyzing Figs. 4 to 12,

it becomes apparent that the EKF estimator accurately follows the real state trajectories with great precision and rapid convergence. Equation (18) allows us to obtain the trajectory of the estimated adhesion force, demonstrating a linear correlation between the load torque and the adhesion force. Fig. 12 shows the estimated adhesion force trajectory. By estimating the longitudinal creep force, it becomes feasible to ascertain the degree of adhesion between the wheel and the rail.

B. Low Speed Performance

To further investigate the proposed method at low speeds, the findings of the estimated stator current, rotor flux, motor speed, and load torque compared to the actual conditions are illustrated in Figs. 13-16. Upon analyzing Figs. 15 and 16, it is evident that the proposed method showcased in this study offers prompt response and precise estimation of speed and torque across the entire low-speed range. In Fig. 15, the reference speed is initially set to 6 rad/s, then altered to -6 rad/s at 4s, and finally adjusted back to 6 rad/s at 14s. Fig. 16 indicates minor estimation errors of similar magnitude. The estimated load torque demonstrates the successful operation of the proposed scheme.
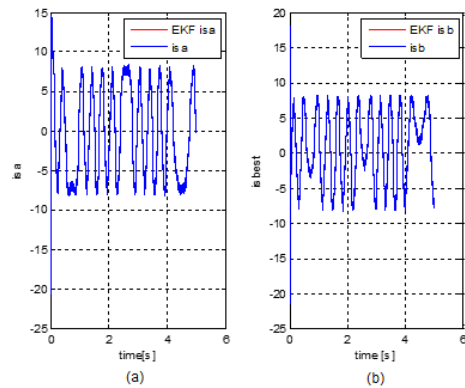

Fig. 13: EKF based estimated and actual motor current trajectories (a) α axis (b) β axis at low speed operation.
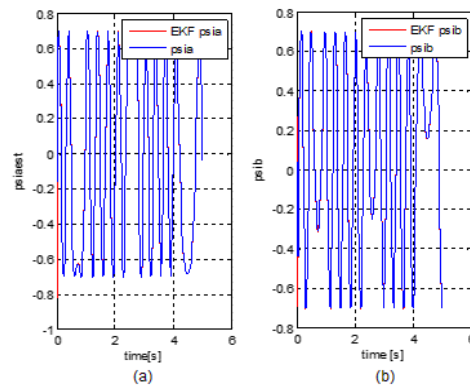

Fig. 14: EKF based estimated and actual rotor flux trajectories (a) α axis (b) β axis at low speed operation.

Fig. 17 displays the trajectory of the adhesion force in low-speed scenarios, which was plotted based on the linear relationship between load torque and adhesion

force. These results confirm the robustness and exceptional tracking capabilities of the estimation approach, even when operating at lower velocities.
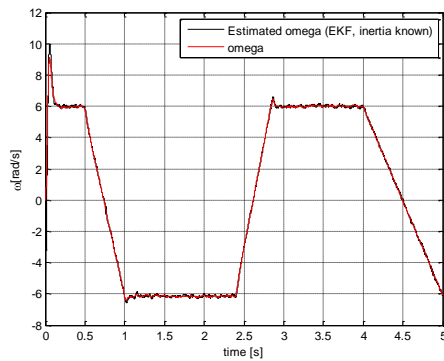

Fig. 15: EKF based estimated and actual trajectories of motor speed at low speed operation.
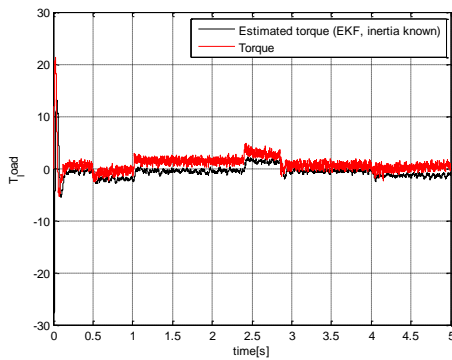

Fig. 16: EKF based estimated and actual trajectories of load torque at low speed operation.
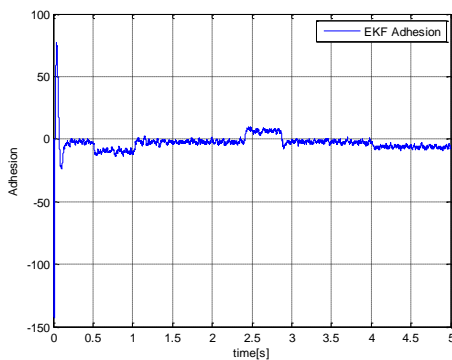

Fig 17: EKF based estimated trajectory of adhesion force at low speed operation.

C. Performance Comparison

As mentioned and considered in subsection 4-1, the estimation of variables with EKF results in good information. For a more detailed investigation and to check the amount of estimation error, and according to subsection 3-2, the performance of the proposed EKF is compared with UKF, validated with Matlab simulation, and comparative analysis is discussed.

In Figs. 18-21 the estimation results of motor current, stator flux, motor speed, and load torque are represented. Both EKF and UKF estimator are used for estimating variables and their outputs compared with the actual situation. As it can be seen, the obtained results present a high degree of convergence, acceptable accuracy, and good estimation of variables in estimating with the EKF estimator. The trajectory of the estimated adhesion in two estimation modes i.e. EKF and UKF is given in Fig. 22. Based on the analysis of the estimation results, it can be deduced that the UKF algorithm, known for its effectiveness in highly-nonlinear systems as per previous research, does not exhibit any advantage over the EKF algorithm when it comes to estimating induction motor parameters and statistics.
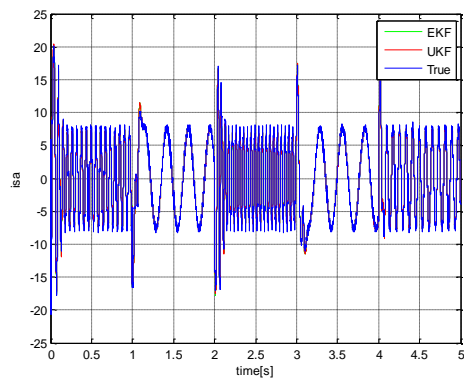

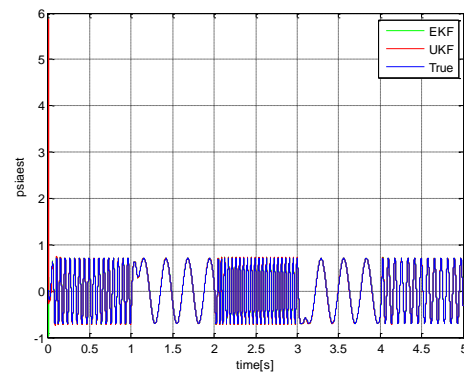Fig. 18: EKF and UKF based estimated and actual motor current trajectories.

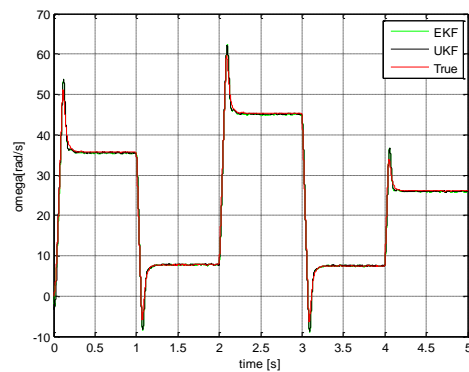Fig. 19: EKF and UKF based estimated and actual rotor flux trajectories.

Fig. 20: EKF and UKF based estimated and actual motor speed trajectories.
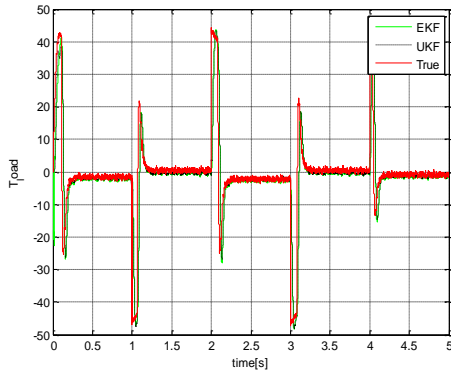
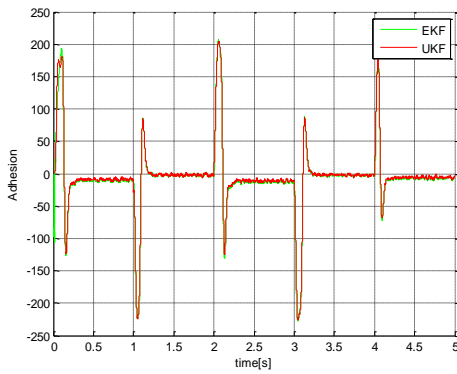Fig. 21: EKF and UKF based estimated and actual load torque trajectories.

Fig. 22: EKF and UKF based estimated adhesion trajectories.

In the following, the trajectories of the estimation error for all mentioned state variables with the UKF and EKF estimation modes are shown in Figs. 23-26. By comparing the obtained results, it is obvious that EKF can estimate variables with high accuracy and partial error in the presence of UKF.

Fig. 26 shows the load torque error in estimating with both EKF and UKF estimators. According to the (18), there is a linear relation between load torque and adhesion force.

Hence, it can be deduced that the EKF exhibits swift responsiveness and provides estimations with minimal margin of error, given the fluctuating adhesion circumstances between the wheel and rail surfaces.
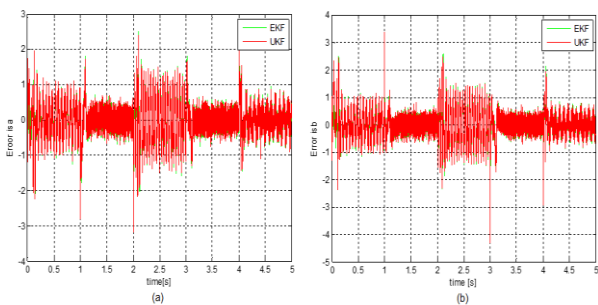

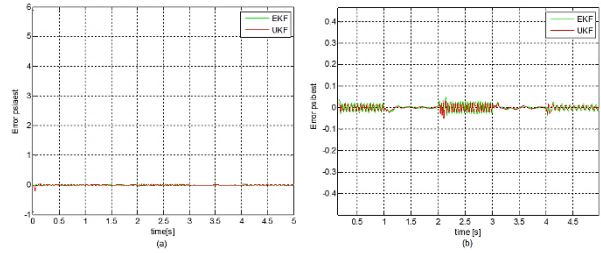Fig. 23: The trajectories of the motor current error (a) α axis (b) β axis.

Fig. 24: The trajectories of the rotor flux error (a) α axis (b) β axis.

To further evaluate the estimation accuracy of the approach, the root mean square error (RMSE) of state variables is shown in Figs. 27-30. By analyzing the Figs, it can be concluded that the RMSE of EKF is smaller than the RMSE of UKF, as a result, the speed estimated by EKF is closer to its actual values.
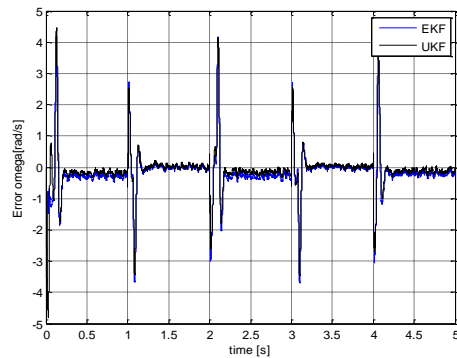
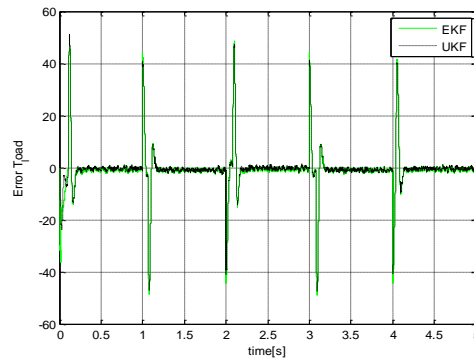

Fig. 25: The trajectory of the motor speed error.

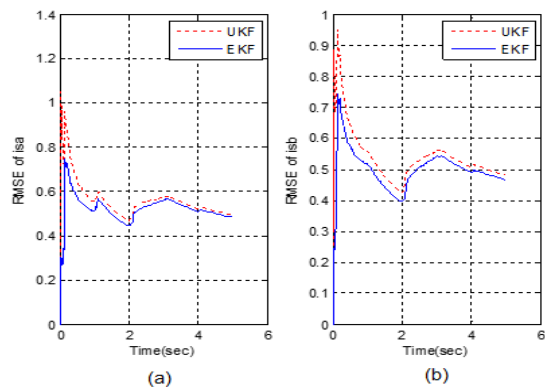Fig. 26: The trajectory of the load torque error.

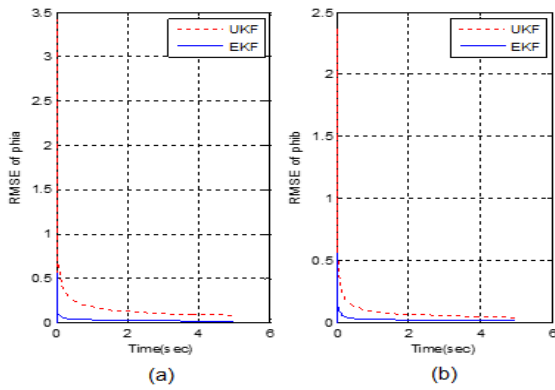Fig. 27: The RMSE of motor current over time (a) in α axis (b) in β axis.

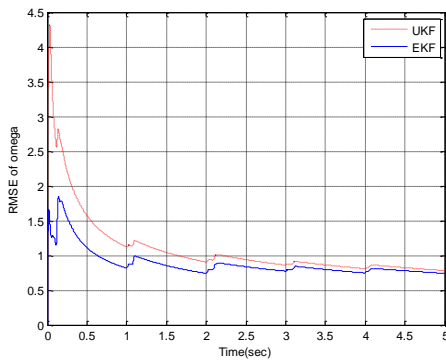Fig. 28: The RMSE of stator flux over time (a) α axis (b) β axis.
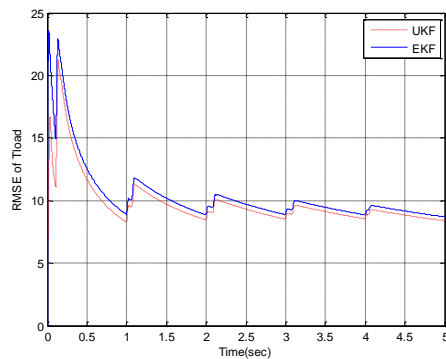

Fig. 29: The RMSE of motor speed over time.

Fig. 30: The RMSE of load torque over time.

Table 3. Running times of EKF and UKF algorithms

Estimator	Execution Time (sec)
EKF	2.6
UKE	9.2

It can be seen in Fig. 30 that the RMSE of load torque with EKF is equal to that of UKF. Therefore, it is the same for adhesion force due to the linear relationship between the load torque and adhesion force. In order to show the difference clearly and better understand the two algorithm performances, the computational cost of methodes is given in Table 3. The results show that the running time of EKF is lower than UKF, which confirm the

superiority of EKF relative to UKF in estimating adhesion force and induction motor parameters.

Conclusion

In this research, an EKF-based condition monitoring is proposed to estimate adhesion force. To assess the efficiency of the estimator, an evaluation was conducted by comparing the estimated motor parameters such as load torque, speed, rotor flux, and stator current in three modes i.e. actual, EKF-based, and UKF-based. Meanwhile, the linear relationship between motor torque and adhesion force was used to determine the adhesion level between the wheel and the rail. The results indicated that the EKF estimator demonstrates prompt responsiveness and accurately estimates the variables, despite the varying adhesion conditions of the wheel-rail contact. The estimator consistently maintains a minimal margin of error. The remarkable thing is that EKF shows its superiority in state and parameter estimation of induction motor and adhesion force since UKF is not able to exhibit its effectiveness for this type of application. Therefore, utilizing such estimator can help to achieve maximum traction, reduce the creepage, and improve the performance of the re-adhesion controller. One major issue with the EKF and UKF lies in the significant impact of the covariance matrices Q and R on the estimation outcomes. If these matrices are chosen badly, the estimation result will be divergent or large estimate errors will be inevitable.

Tuning of Q and R is necessary to yield the best estimations. Changing these two matrices affects both the steady-state and transient duration operation of the estimator. When the value of Q increases, it indicates the presence of significant disturbances or uncertainties in the machine model. Consequently, the Kalman gain is augmented, resulting in a faster performance of the estimator during the transitional phase. On the other hand, increasing R means that noise measurements are strong and the noise will be weighted less by estimator, which leads to Kalman gain decrease and gives us a slower transient performance. To enhance the performance, accuracy, and stability of the estimator, it is imperative to employ various tuning algorithms. In our upcoming endeavors, we will focus on implementing these algorithms and give particular attention to developing a real-time system.

Author Contributions

M. Moradi collected the data, carried out the analysis and wrote paper, R.Havangi wrote the paper ,interpreted the results and supervised the research.

Acknowledgment

Conflict of Interest

The authors declare no potential conflict of interest regarding the publication of this work. In addition, the ethical issues including plagiarism, informed consent, misconduct, data fabrication and, or falsification, double publication and, or submission, and redundancy have been completely witnessed by the authors.

Abbreviations

a and b: Semi-axis length of the contact patch

B and D: Reduction factors

C_{11}: Kalker coefficient

C_v: Viscous friction

F_a: Adhesion force

F_N: Normal force between the wheel and rail

G: Shear module

$I_{s\alpha}$ and $I_{s\beta}$: $\alpha-\beta$ axis stator currents

c_1 and c_2: Self-recognition and social component coefficients

J_{eqv}: Equivalent moment of inertia

J_g: Gearbox moment of inertia

J_x: Wheelset axle moment of inertia

J_{wR} and J_{wL}: Right and left wheel moment of inertia

k_A and k_S: Reduction factors in the adhesion and slip area

L_m: Mutual inductance

L_r and L_s: Rotor and stator self-inductance

n_i: Gear reduction ratio

n_p: Number of the pole pairs

N: Number of unknown variables or number of samples

P_i: Previous best position of each particle

Q and R: Process and measurement noise covariance matrixes

r: Wheel radius

R_r and R_s: Rotor and stator resistance

n_i: Gear reduction ratio

T_m: Motor torque

T_L: Load torque

V: Longitudinal velocity

$v(t)$ and $w(t)$: Measurement and process noise

V_i: Particle velocity

w: Inertia weight factor

X_i: i[th] particle position

$\psi_{r\alpha}$ and $\psi_{r\beta}$: $\alpha-\beta$ axis rotor flux

μ_f: Traction coefficient

σ: Leakage coefficient

ϵ: Gradient of tangential stress

ξ: Creepage between the wheel and rail

ω_m: Motor angular velocity

ω_w: Wheel angular velocity

References

[1] C. Schwarz, A. Keck, "Simultaneous estimation of wheel-rail adhesion and brake friction behaviour," IFAC, 53: 8470-8475, 2020.

[2] R. Lewis, G. Trummer, K. Six, J. Stow, H. Alturbeh, P. Shackleton, B. Bryce, L. Buckley Johnstone, "Leaves on the line: Characterizing leaf based low adhesion on railway rails," Tribol. Int., 185: 108529, 2023.

[3] H. Chen, T. Furuya, S. Fukagai, S. Saga, J. Ikoma, K. Kimura, J. Suzumura, "Wheel slip/slide and low adhesion caused by fallen leaves," Wear, 446-447: 203187, 2020.

[4] M. Watson, B. White, J. Lanigan, T. Slatter, R. Lewis, "The composition and friction reducing properties of leaf layers," Proc. Math. Phys. Eng. Sci., 476 (2239), 2020.

[5] J. Zhou, M. Wu, C. Tian, et al., "Experimental investigation on wheel–rail adhesion characteristics under water and large sliding conditions," Ind. Lubric. Tribol., 73(2): 366-372, 2021.

[6] Y. Lyu, E. Bergseth, U. Olofsson "Open system tribology and influence of weather condition," Sci. Rep. , 6: 32455, 2016.

[7] M. Harmon, R. Lewis "Review of top of rail friction modifier tribology," Tribol. Mater. Surface Interfac., 10(3): 150-162, 2016.

[8] M. Shen., Y. Qin, D. Ji, et al. "Role of ambient temperature in the adhesion and damage characteristics of wheel/rail interface during rolling-sliding contact," Wear, 506-507: 204458, 2022.

[9] H. Chen, H. Tanimoto, "Experimental observation of temp-erature and surface roughness effects on wheel/rail adhesion in wet conditions," Int. J. Rail Transport., 6(2): 101-112, 2018.

[10] U. Olofsson, Y. Lyu, "Open system tribology in the wheel–rail contact—a literature review," Appl. Mech. Rev. 69(6): 60803, 2017.

[11] I. Yasuoka, T. Henmi, Y. Nakazawa, I. Aoyama, "Improvement of re-adhesion for commuter trains with vector control traction inverter," in Proc. Power Conversion Conference - PCC '97, 1: 51-56, 1997.

[12] Y. Matsumoto, N. Eguchi, A. Kawamura, "Novel re-adhesion control for train traction system of the "Shinkansen" with the estimation of wheel-to-rail adhesive force," in Proc. IECON'01. 27th Annual Conference of the IEEE Industrial Electronics Society (Cat. No.37243), 2: 1207-1212, 2001.

[13] K. Zhao, P. Li, Ch. Zhang, J. He, Y. Li, T. Yin, "Online accurate estimation of the wheel-rail adhesion coefficient and optimal adhesion antiskid control of heavy-haul electric locomotives based on asymmetric barrier lyapunov function," J. Sensors, 2018: Article ID 2740679, 2018.

[14] R. Bibi, B. S. Chowdry, R. A. Shah, "PSO based localization of multiple mobile robots employing LEGO EV3," in Proc. 2018 International Conference on Computing, Mathematics and Engineering Technologies (iCoMET): 1-5, 2018.

[15] S. Shrestha, Q. Wu, M. Spiryagin, "Review of adhesion es-timation approaches for rail vehicles," Int. J. Rail Transport., 7(2): 79-102, 2019.

[16] X. Fang, S. Lin, Z. Yang , F. Lin, H. Sun, L. Hu "Adhesion control st-rategy based on the wheel-rail adhesion state observation for high-speed trains," Electronics, 7(5): 70, 2018.

J. Electr. Comput. Eng. Innovations, 12(1): 271-282, 2024

281

[17] B. Liu, T. X. Mei, S. Bruni, "Design and optimisation of wheel–rail profiles for adhesion improvement," Veh. Syst. Dyn., 54(3): 429-444, 2016.

[18] Y. Chen, H. Dong, J. Lu, X. Sun, L. Guo, "A super-twisting-like algorithm and Its application to train operation control with optimal utilization of adhesion force," IEEE Trans. Intell. Transpor. Syst., 17(11): 3035-3044, 2016.

[19] M. Yamashita, T. Soeda, "Anti-slip re-adhesion control method for increasing the tractive force of locomotives through the early detection of wheel slip convergence," in Proc. 17th European Conference on Power Electronics and Applications: 1-10, 2015.

[20] R. Rizzo, D. Iannuzzi, "Indirect friction force identification for application in traction electric drives," Math. Comput. Simul., 60(3-5): 379-387, 2002.

[21] I. Hussain, T. X. Mei, R. T. Ritchings, "Estimation of wheel– rail contact conditions and adhesion using the multiple model approach," Veh. Syst. Dyn., 51(1): 32-53, 2013.

[22] G. Charles, R. Goodall, R. Dixon, "Model-based condition monitoring at the wheel-rail interface," Veh. Syst. Dyn., 46(1): 415-430, 2008.

[23] F. Orderud, "Comparison of kalman filter estimation approa-ches for state space models with nonlinear measurements," in Proc. Scand. Conf. Simul., 194: 157-162, 2005.

[24] Y. Zhao, B. Liang, "Re-adhesion control for a railway single wheelset test rig based on the behaviour of the traction motor," Veh. Syst. Dyn., 51(8): 1173-1185, 2013.

[25] S. Wang, J. Xiao, J. Huang, H. Sheng, "Locomotive wheel slip detection based on multi-rate state identification of motor load torque,"J. Franklin Inst., , 353(2): 521-540, 2016.

[26] P. D. Hubbard, C. Ward, R. Dixon, R. Goodall, "Verification of model based adhesion estimation in the wheel-rail interface," Chem. Eng. Trans., 33: 757-762, 2013.

[27] A. Onat, P. Voltr, M. Lata, "An unscented Kalman filter-based rolling radius estimation methodology for railway vehicles with traction," Proc. Inst. Mech. Eng., Part F: J. Rail Rapid Transit, 232(6): 1686-1702, 2018.

[28] S. Jafarzadeh, C. Lascu, M. Fadali, "Square root unscented Kalman Filters for state estimation of induction motor drives," IEEE Trans. Ind. Appl., 49(1): 92-99, 2013.

[29] S. Jafarzadeh, C. Lascu, M. Fadali, "State estimation of induction motor drives using the unscented Kalman filter," IEEE Trans. Ind. Electron., 59(11): 4207-4216, 2012.

[30] B. Akin, U. Orguner, A. Ersak, M. Ehsani, "Simple derivative free nonlinear state observer for sensorless AC drives," IEEE/ASME Trans. Mech., 11(5): 634-643, 2006.

[31] M. Barut, S. Bogosyan, M. Gokasan, "Speed-sensorless estimation for induction motors using extended Kalman filters," IEEE Trans. Ind. Electron., 54(1): 272-280, 2007.

[32] M. Spiryagin, P. Wolfs, C. Cole, V. Spiryagin, "Design and simulation of heavy haul locomotives and trains," CRC Press, Boca Raton, FL, USA, 2016.

[33] O. Polach, "A fast wheel-rail forces calculation computer," Veh. Syst. Dyn. Suppl., 33(1): 728-739, 1999.

[34] J. Kalker, "On The rolling contact of two elastic bodies in the presence of dry friction," Wear, 11: 303, 1967.

Biographies

Maryam Moradi received her B.S. degree in Control Engineering from Gonabad Azad University, Gonabad, Iran in 2008, and her M.S. degree in Telecommunications Engineering from the Faculty of Engineering at the University of Sistan and Baluchestan, Zahedan, Iran in 2015. Since 2018, she has been a Ph.D. student in Control Engineering at the Faculty of Engineering, the University of Birjand, Birjand, Iran. In 2019, she joined the University of Applied Sciences & Technology as a teacher.

- Email: m_moradi@birjand.ac.ir
- ORCID: 0009-0007-0635-6867
- Web of Science Researcher ID: NA
- Scopus Author ID: NA
- Homepage: NA

Ramazan Havangi received his M.S. and Ph.D. degrees from the K.N. Toosi University of Technology, Tehran, Iran in 2003 and 2012, respectively. He is currently an Associate Professor of control systems with the Department of Electrical and Computer Engineering at the University of Birjand, Birjand, Iran. His main research interests are inertial navigation, integrated navigation, estimation and filtering, evolutionary filtering, simultaneous localization and mapping, fuzzy, neural network, and soft computing.

- Email: : Havangi@Birjand.ac.ir
- ORCID: 0000-0001-5711-3127
- Web of Science Researcher ID: NA
- Scopus Author ID: NA
- Homepage: https://cv.birjand.ac.ir/havangi/fa